JOURNAL OF SPACECRAFT AND ROCKETS
Vol. 40, No. 3, May–June 2003

Methodology for Turbulence Model Validation: Application to Hypersonic Flows

Christopher J. Roy* and Frederick G. Blottner†
Sandia National Laboratories, Albuquerque, New Mexico 87185

Hypersonic transitional flows over a flat plate and a sharp cone are studied using four turbulence models: the one-equation eddy viscosity transport model of Spalart–Allmaras, a low-Reynolds-number k–ε model, the Menter k–ω model, and the Wilcox k–ω model. A framework is presented for the assessment of turbulence models that includes documentation procedures, numerical accuracy, model sensitivity, and model validation. The accuracy of the simulations is addressed, and the sensitivities of the models to grid refinement, freestream turbulence levels, and wall y^+ spacing are presented. The flat-plate skin-friction results are compared to the well-established laminar and turbulent correlations of Van Driest. Correlations for the sharp cone are discussed in detail. These correlations, along with recent experimental data, are used to judge the validity of the simulation results for skin friction and surface heating on the sharp cone. The Spalart–Allmaras model performs the best with regards to model sensitivity and model accuracy, whereas the Menter k–ω model also performs well for these zero pressure gradient boundary-layer flows.

Nomenclature

C_μ	=	turbulence modeling constant, 0.09
c_f	=	skin-friction coefficient
c_p	=	specific heat at constant pressure, J/kg · K
f	=	generic solution variable
H	=	total enthalpy, J/kg
h	=	specific enthalpy, J/kg
k	=	specific turbulent kinetic energy, m^2/s^2
M	=	Mach number
m	=	Van Driest correlation parameter
P	=	turbulent kinetic energy production term, $\tau_{ij}(\partial\mu_i/\partial x_j)$
Pr	=	Prandtl number, 0.71
Pr_T	=	turbulent Prandtl number, 1.0
p	=	pressure, N/m^2
q	=	heat flux, W/m^2
Re	=	Reynolds number based on freestream conditions
r_f	=	recovery factor
St	=	Stanton number
s	=	surface distance from stagnation point, m
T	=	temperature, K
T_u	=	freestream turbulence intensity, %
u	=	axial velocity, m/s
u_τ	=	friction velocity, $\sqrt{(\tau_w/\rho)}$
V	=	velocity magnitude, m/s
x	=	axial coordinate, m
y	=	wall normal direction, m
y^+	=	wall normal direction in wall coordinates, $u_\tau y/\nu$
γ	=	ratio of specific heats
ε	=	specific dissipation rate, m^2/s^3
θ	=	momentum thickness, m
μ	=	absolute viscosity, Ns/m^2
ν	=	kinematic viscosity, m^2/s
ρ	=	density, kg/m^3
τ	=	shear stress, N/m^2
τ_{ij}	=	Reynolds stress tensor, N/m^2
ω	=	specific turbulent frequency, 1/s

Subscripts

aw	=	adiabatic wall value
c	=	cone value
e	=	edge condition
fp	=	flat-plate value
i, j	=	indices for tensor notation
k	=	mesh level 1, 2, 3, fine to coarse
t	=	turbulent quantity
w	=	wall value
∞	=	freestream value

Presented as Paper 2001-0210 at the AIAA 39th Aerospace Sciences Meeting, Reno, NV, 8–11 January 2001; received 10 May 2002; revision received 26 September 2002; accepted for publication 30 October 2002.

*Senior Member of Technical Staff, Mail Stop 0825, P.O. Box 5800; cjroy@sandia.gov. Senior Member AIAA.

†Distinguished Member of Technical Staff, Mail Stop 0825, P.O. Box 5800; fgblott@sandia.gov. Fellow AIAA.

Introduction

AN effort is currently underway at Sandia National Laboratories to review and assess existing turbulence models for hypersonic flows. These flows generally consist of laminar, transitional, and turbulent regions. This study deals with transition by the a priori specification of a transition point. The prediction of transition onset and extent is a challenging task and is beyond the scope of the current work. The main goal of this study is to evaluate several turbulence models for two simple, zero pressure gradient, attached boundary-layerflows: a flat plate and a sharp cone. Although a large amount of experimental data exist for these cases, correlations are also available that incorporate much of the data. Van Driest developed correlations for the skin friction and heating on a flat plate for both laminar[1] and turbulent[2] flow. These correlations are based on boundary-layer theory and have been confirmed by numerous experiments. Van Driest[3] and White[4] have also developed correlations for skin friction and heating on sharp cones. These correlations were revisited in the Appendix of Ref. 5.

A secondary goal of this study is to develop a framework for the assessment of turbulence models. The assessment methodology presented herein is influenced heavily by the work of Marvin[6] and Huang.[7] The proposed assessment framework includes guidelines for documentation, model sensitivities, and model validation. In addition, a significant effort has been made to estimate the numerical accuracy of the simulations. The procedures for determining numerical accuracy are based on earlier work by the authors.[8,9]

The computational fluid dynamics code used herein is the Sandia Advanced Code for Compressible Aerothermodynamics Research and Analysis (SACCARA). The SACCARA code was developed from a parallel distributed memory version[10,11] of the INCA code, originally written by Amtec Engineering. This code has been

developed to provide a massively parallel, three-dimensional compressible fluid mechanics/aerothermodynamics analysis capability for transonic and hypersonic flows.

Four turbulence models are examined in the current work. The first turbulence model is the one-equation Spalart–Allmaras eddy-viscosity model,[12,13] which has a robust numerical formulation and has shown promising results for a wide variety of flows. The second model is the standard k–ε model,[14] which uses low-Reynolds-number damping functions[15] near solid walls. The third model is Menter's hybrid model,[16] which switches from a k–ε formulation in the outer flow to a k–ω formulation near solid walls. The fourth model is Wilcox's improved version[14] of his earlier k–ω turbulence model.[17]

Two cases are used to investigate the performance of the one- and two-equation turbulence models, both of which are zero pressure gradient flows. The first case is the flow over a flat plate at Mach 8. The skin friction along the flat plate is used to judge the accuracy of the predictions through comparisons with the well-established laminar and turbulent correlations of Van Driest.[1,2] The second case is the Mach 8 flow over a sharp cone. Supersonic and hypersonic flows over a sharp cone are of interest because the flow properties at the edge of the boundary layer are approximately constant along the cone. Thus, the sharp cone is an extension of the flat-plate geometry and is basic to the understanding of turbulent boundary-layer flows and other flow geometries. This geometry is well suited for wind-tunnel testing and avoids the two-dimensional/three-dimensional issues such as side-wall effects that can occur in flat-plate flows. From a computational point of view, this geometry is not ideal because the singularity at the sharp tip can make it difficult to obtain accurate numerical solutions.

Two recent validation studies for compressible boundary layers have been performed. Huang et al.[18] compared various low-Reynolds-number k–ε models, as well as the Wilcox k–ω model,[17] to the Van Driest[2] transformed velocity profile in a number of compressible boundary-layer flows. They showed that, particularly in the case of the k–ε models, the wake component of velocity for compressible boundary layers was overpredicted and, thus, would be expected to underpredict the skin friction. This conclusion is not supported by the results of the current study. Kral et al.[19] examined a variety of algebraic, one-equation, and two-equation turbulence models for a number of complex two-dimensional and three-dimensional compressible flows. In general, the algebraic models performed poorly in complex flows with boundary-layer separation, whereas the one- and two-equation models each were found to have their own strengths and weaknesses. In addition, a production limiter for the turbulent kinetic energy (similar to that used in the current work) was found to improve greatly the accuracy of the model predictions.

A number of high-speed transitional flow experiments have been carried out on the sharp cone geometry. The earlier database for sharp cones has been reviewed by Bertin et al.[20] One of the earlier wind-tunnel investigations on the skin friction and heat transfer on a sharp cone at a freestream Mach number of 7.9 was performed by Chien.[21] A published workshop edited by by Desideri et al.[22] used the sharp cone as one of the hypersonic turbulent flow problems to be solved by participants. The original data for the problem have been developed further with the data obtained in the Imperial College number 2 gun tunnel at a Mach number of 9.26. Experiments have been performed by Lin and Harvey[23] and Hillier et al.[24] In the latter case, blunt cones have also been investigated. Transition on a sharp cone in a Mach 3.5 low-disturbance tunnel has been investigated by Chen et al.[25] Heat transfer measurements on sharp cones with an afterbody that is a flare or ogive have been performed by Kimmel,[26,27] with the baseline model consisting of a 7-deg half-angle sharp cone with a freestream Mach number of 7.93.

One of the problems with the sharp cone is the lack of a completely adequate theory-based correlation of the experimental data to use as a benchmark solution. For laminar flow, the skin friction and heat transfer for a flat plate are multiplied by $\sqrt{3}$ to obtain the cone values. There does not appear to be a well-established approach to transform the turbulent flat plate results to the cone. A correlation of the heat transfer on axisymmetric flight vehicles with flat-plate relations has been investigated by Zoby and Sullivan,[28] and an additional correlation, including ground-test data, has been investigated by Zoby and Graves.[29] The former includes six references for experimental data on sharp cones, where the Mach number varies from 2.0 to 4.2. An assessment of the theoretical correlations for sharp cones was given in Ref. 5.

The conditions chosen for the Mach 8 sharp cone flow studied herein correspond to the experiment conducted by Kimmel,[26,27] which contains surface heat transfer data. These data, along with the correlations for surface heat transfer and skin friction developed by Van Driest[3] and White,[4] are used to assess the accuracy of the model predictions.

Turbulence Model Assessment Methodology

One of the goals of this work is to develop criteria for assessing the turbulence models. Six criteria are listed for assessing the models. The first three criteria focus on the thorough documentation of the model evaluation efforts. Details of the flow case and the models used must be given in enough detail so that the results are reproducible by other researchers. The last three criteria list the specific standards for evaluating the models. The turbulence models should be evaluated by first establishing the numerical accuracy of the simulations and then by examining model sensitivities and validation comparisons to experimental data.

Criterion 1: Cases Examined

Details of (or references to) the specific flow problem examined should be given, including flowfield geometry and relevant physics, for example, ideal gas vs equilibrium thermochemistry, transport properties, etc. All required boundary conditions should be listed, including inflow and outflow conditions, solid-wall boundary conditions for temperature, incoming boundary-layer thickness, freestream turbulence intensities, a measure of the freestream turbulence dissipation rate, etc. One of the difficulties encountered in the specification of computational boundary conditions is that the level of information required may not be characterized in the experiment. For example, the large-eddy simulation of a turbulent flow may require spatial and temporal evolution information at the boundaries. It should be clearly stated whether the flow is fully turbulent or transitional. Finally, the data available for model validation should be given, for example, feature location, surface quantities, turbulent field profiles, etc.

Criterion 2: Turbulence Models Examined

It should be clearly stated which form of the turbulence model is employed. It is strongly suggested that the standard model constants be used to build on earlier turbulence model validation efforts. Where applicable, the form of the low-Reynolds-number wall damping functions used should be stated. The treatment of the near-wall regions should also be listed, that is, integration to the wall or wall functions.

Criterion 3: Model Implementation Issues

The form of the governing equations should be given. For example, different results may be found when employing the full Navier–Stokes, thin-layer Navier–Stokes, parabolized Navier–Stokes, viscous shock-layer equations, or boundary-layer equations. The boundary conditions employed in the simulation, including both flow properties and turbulence quantities, should be specified. Finally, any limiting of the turbulence quantities should be discussed. For example, limiting of the ratio of production to dissipation of turbulent kinetic energy to some ratio, for example, $P/\rho\varepsilon \leq 5$, is often used. In addition, realizeability constraints on the turbulence variables and/or normal turbulent stresses[30] should also be discussed.

Criterion 4: Efforts to Establish Numerical Accuracy

The numerical accuracy (or discretization error) of the simulations is an important factor when comparing to experimental data; for example, if the numerical accuracy of pressure distributions are estimated to be $\pm 20\%$, then clearly one should not expect to get agreement with experimental data within 5%. The first step toward determining the accuracy of the simulations is code verification, that is, building confidence that the code is solving the governing equations correctly. Code verification can be performed by comparison

of the code results to exact solutions to the governing equations, highly accurate numerical solutions (or benchmark solutions), or by the method of manufactured solutions.[31,32] Once one has confidence that the code is verified, then the accuracy of the individual solutions must be verified. Solution accuracy includes assessing the errors due to incomplete iterative convergence[8,9] for steady-state problems, temporal convergence for unsteady problems, and grid convergence. Methods for estimating the grid convergence errors based on systematic grid refinement[9,33] tend to be the most reliable and are applicable to any type of discretization, including finite difference, finite volume, and finite element. Grid convergence error estimates for hypersonic flows are complicated by the presence of shock waves, which tend to reduce the spatial order of accuracy to first order,[34,35] regardless of the nominal order of the spatial discretization scheme.

Criterion 5: Turbulence Model Sensitivities

Model sensitivity studies should be performed to determine practical guidelines for model use. A systematic study of the effects of the freestream turbulence levels on the numerical predictions should be performed. The normal spacing at the wall y^+ should also be varied to test model robustness and accuracy for both integration to the wall and wall functions. In addition to establishing the solution accuracy, a mesh refinement study can also be used to determine a given turbulence model's sensitivity to the mesh density.

Criterion 6: Turbulence Model Validation Results

Model validation results should be presented in a quantitative manner, rather than qualitatively. For example, the percent difference between the predictions and experiment should be plotted or explicitly stated. Experimental error bounds should be given for all measurements used for validation. These error bounds should include contributions from instrument uncertainty, experimental run-to-run uncertainty, physical model alignment uncertainty, flowfield nonuniformities, etc.[36]

Flowfield Solver

The SACCARA code is used to solve the compressible Navier–Stokes equations for conservation of mass, momentum, energy, and turbulence transport in either two-dimensional or axisymmetric form. The governing equations are discretized using a cell-centered finite volume approach. A finite volume form of Harten's[37] and Yee's[38] symmetric total variation diminishing scheme is employed. This flux scheme is second-order accurate and reduces to a first-order Roe-type scheme[39] in regions of large gradients, that is, shocks, based on a minmod limiter. The viscous terms are discretized using central differences.

The SACCARA code employs a massively parallel distributed memory architecture based on multiblock structured grids. The solver is a lower–upper symmetric Gauss–Seidel scheme based on the works of Yoon and Jameson,[40] Yoon and Kwak,[41] and Peery and Imlay,[42] which provides for excellent scalability up to thousands of processors.[43] The SACCARA code has been used to obtain solutions for a wide variety of compressible flow problems.[8–11,44–46] The simulations presented herein were run using a 400-MHz Sun workstation. Typical CPU times to reach convergence for the fine mesh two-equation model runs were approximately 18 h for each flat plate case and 11 h for each sharp cone case. The Spalart–Allmaras model[12,13] CPU times were somewhat shorter.

All flow solutions were initialized by applying the freestream conditions over the entire domain. The governing equations were then advanced in pseudotime until a steady-state solution was obtained. The Courant–Friedrichs–Lewy (CFL) number at the beginning of the simulations was set to 0.1. This value was then geometrically ramped up by a factor of 1.01 until the CFL number reached 1×10^6. For the k–ω models, the sharp cone simulations were run with zero eddy viscosity for the first 1000 iterations and then allowed to transition to turbulent flow downstream of the transition location thereafter. This procedure was required due to instabilities that arose when the shock moved off of the body and through the turbulent boundary layer.

Turbulence Models

Transition Method

The current method for specifying transition from laminar to turbulent flow in the SACCARA code is through analogy with the turbulence intermittency approach. The turbulence transport equations are solved over the entire domain, with a user-defined transition plane specified. Upstream of this plane, the effective viscosity is simply the laminar value, whereas downstream the effective viscosity is the sum of the laminar and turbulent viscosities. An advantage of this approach is that the turbulence transport equations are solved over the whole domain, thus promoting turbulent behavior downstream of the transition plane. In contrast, if the turbulence source terms are simply turned on after the transition plane, the turbulence model may not transition to turbulent flow until farther downstream, depending on the freestream turbulence values. A disadvantage of the current approach is that a discontinuity in the total viscosity (laminar plus turbulent) may occur at the transition plane. Note that the transition location is specified a priori and not modeled, with the current method admitting sharper gradients in the transitional region.

Spalart–Allmaras Model[12,13]

The Spalart–Allmaras[12,13] one-equation turbulence model is examined. This model requires the solution of a single transport equation for the eddy viscosity. The Spalart–Allmaras model has proven to be a numerically robust approach, and generally good results have been demonstrated for a wide variety of flows. The density gradient term that arises from the transformation from the original incompressible formulation in substantial derivative form is omitted. See Refs. 8 and 9 for details. In addition, the boundary-layer trip terms f_{t1} and f_{t2} are omitted.

Low-Reynolds-Number k–ε Model

The standard k–ε model,[14] although providing good results for shear flows, is not appropriate for wall-bounded flows. The low-Reynolds-number modification of Nagano and Hishida[15] is used to allow integration to solid walls. The current implementation uses the incompressible form of the turbulence production term P, which omits terms containing the divergence of velocity. This production term is limited to 10 times the dissipation, that is, $P \leq 10\rho\varepsilon$. All other turbulence models employ the compressible form of the production term.

Menter k–ω Model[16]

The Menter k–ω model[16] is a hybrid model that uses a blending function to combine the best aspects of both the k–ω and the k–ε turbulence models. Near solid walls, a k–ω formulation is used that allows integration to the wall without any special damping or wall functions. Near the outer edge of the boundary layer and in shear layers, the model blends into a transformed version of the k–ε formulation, thus, providing good predictions for free shear flows. This model also shows less sensitivity to freestream turbulence quantities than other k–ω formulations. The turbulent kinetic energy production term is limited to 10 times the dissipation ($P \leq 10\beta^*\rho k\omega$).

Wilcox k–ω Model[14]

The second k–ω formulation examined is a modification to an earlier Wilcox k–ω model.[17] The updated version[14] was developed to improve predictions for free shear layers and to reduce the solution sensitivity to freestream w values. This version is referred to as the Wilcox k–ω model[14] in the current study. The turbulent kinetic energy production term is also limited to 10 times the dissipation, similar to the Menter k–ω model.[16]

Solid-Wall Boundary Conditions

For the Spalart–Allmaras model,[12,13] the transported eddy viscosity is set to zero at solid walls. For the three two-equation models, the turbulent kinetic energy k is specified to be zero at the surface. The boundary condition for the specific dissipation rate is approximated by setting ε to zero at solid surfaces. For the k–ω models, the

omega value for the first cell off the wall ω_1 is set to

$$\omega_1 = \frac{6\nu}{\beta_0(\Delta y)^2} \tag{1}$$

where Δy is the distance from the cell center to the wall and $\beta_0 = 9/125$ for the Wilcox model[14] and $\beta_0 = 3/40$ for the Menter model.[16] The wall value is set to

$$\omega_w = 10\frac{6\nu_w}{\beta_0(\Delta y)^2} \tag{2}$$

The ghost cell (first cell within the boundary) value for w is set so that the second derivative of w at the wall is zero, that is,

$$\left.\frac{\partial^2\omega}{\partial y^2}\right|_w = 0 \tag{3}$$

Transitional Flow Cases

Flat Plate

Flow over a flat plate has been chosen as the first test case, to illustrate the behavior of the transitional flow results obtained with the one- and two-equation turbulence models. The test case consists of Mach 8 flow over a flat plate with a wall temperature of $T_w = 1000$ K and freestream conditions corresponding to an altitude of 15 km (Ref. 47). For this case, the temperature in the flow is sufficiently low such that the perfect gas assumption with $\gamma = 1.4$ is appropriate. Sutherland's law for air was used for the molecular viscosity. The transition location was specified as $x = 0.12$ m from the leading edge to provide a significant region of fully developed turbulent flow.

Freestream Flow Conditions

The freestream conditions for the flat plate case are presented in Table 1. The method for determining the freestream turbulence properties is given as follows. For the two-equation models, the specification of a freestream turbulence intensity T_u is used to determine the turbulent kinetic energy in the freestream from

$$k = (1.2/2)[(T_u/100)V_\infty]^2 \tag{4}$$

where, for example, $T_u = 10$ corresponds to a freestream turbulence intensity of 10%. The dissipation variable is determined by specifying the ratio of turbulent to laminar viscosity, μ_t/μ, that is,

$$\varepsilon = \frac{C_\mu \rho k^2/\mu}{\mu_t/\mu} \tag{5}$$

or

$$\omega = (\rho k/\mu)/(\mu_t/\mu) \tag{6}$$

For the Spalart–Allmaras model,[12,13] the eddy viscosity is simply found from laminar viscosity μ and the μ_t/μ ratio. The baseline values for the flat plate are $T_u = 1\%$ and $\mu_t/\mu = 1$. These values are used for the flat plate throughout this paper unless otherwise stated.

Table 1 Flow conditions for the Mach 8 flat plate

Parameter	Value
M_∞	8
Re	3.24×10^7/m
p_∞	1.21114×10^4 N/m^2
T_∞	216.65 K
ρ_∞	0.19475 kg/m^3
V_∞	2360.54 m/s
μ_∞	1.4216×10^{-5} kg/ms
$\mu_{t\infty}$	1.4216×10^{-5} kg/ms
k_∞	334.3 m^2/s^2
ε_∞	1.382×10^6 m^2/s^3
ω_∞	4.594×10^6 1/s
T_w	1000 K

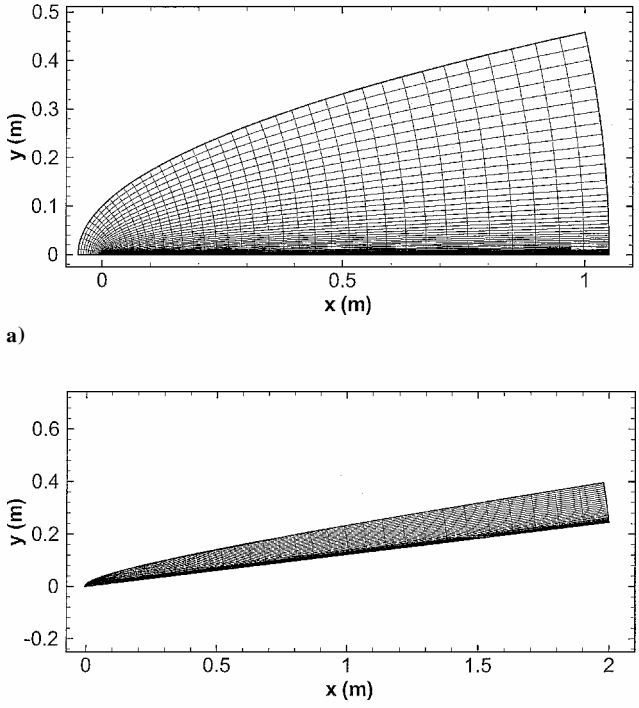

Fig. 1 Computational mesh for a) the flat plate (every other point shown) and b) the sharp cone (every fourth point shown).

Computational Mesh

A parabolic mesh was used around the flat plate as shown in Fig. 1a. This mesh topology mitigates the effects of the leading-edge singularity by clustering points in this region and provides a set of well-defined boundary conditions to apply at the solution boundaries. Details of the method used to generate the parabolic mesh are given in Refs. 8 and 9. Most of the results have been obtained with a fine mesh of 80×160 cells (80 cells along the plate surface). Coarser meshes of 40×80 and 20×40 cells were also used to show that the 80×160 mesh provides results sufficiently accurate for assessing the models. The coarser meshes were generated from the fine mesh by eliminating every other grid line in each direction. Maximum y^+ values (measured from the wall to the nearest cell center) of approximately 0.1 were used for the fine mesh in the turbulent flow region. The sensitivity of the turbulence model results to wall y^+ spacing will also be addressed.

Sharp Cone

Flow over a sharp cone with a half-angle of 7 deg has been chosen as the second test case to illustrate the behavior of the laminar/turbulent flow results obtained with the turbulence models. The flow conditions correspond to a wind-tunnel test performed by Kimmel.[26,27] Transition occurs at approximately 0.5 m downstream of the nose. The gas is air and the temperatures are such that the perfect gas assumption with $\gamma = 1.4$ is again appropriate. Because of the low freestream temperatures, Keyes viscosity model[48] was used to determine the freestream conditions from the Reynolds number quoted in the experiment. The temperatures in the boundary layer are sufficiently high such that Sutherland's law is used for all simulations.

Freestream Flow Conditions

The flow conditions for the sharp cone are presented in Table 2. The baseline freestream turbulence values for the sharp cone are $T_u = 1\%$ and $\mu_t/\mu = 10$ [Eqs. (4–6)]. The values were chosen to ensure that all models provided turbulent solutions downstream of the transition plane. These values are used for the sharp cone throughout this paper unless otherwise stated.

Table 2 Flow conditions for the Mach 8 sharp cone

Parameter	Value
M_∞	7.93
Re_∞	6.6×10^6/m
p_∞	331.02 N/m^2
T_∞	53.18 K
ρ_∞	0.02169 kg/m^3
V_∞	1159.3 m/s
μ_∞	3.45×10^{-6} kg/ms
$\mu_{t\infty}$	3.45×10^{-5} kg/ms
k_∞	80.64 m^2/s^2
ε_∞	3.678×10^5 m^2/s^3
ω_∞	5.068×10^4 1/s
T_w	303.24 K

Computational Mesh

A parabolic mesh was used for the sharp cone with 160×160 cells (Fig. 1b). Details of the mesh generation procedure are given in Ref. 5 To assess the spatial error of the surface distributions, a medium mesh of 80×80 cells and a coarse mesh of 40×40 cells were generated by eliminating every other grid line from the fine mesh in each direction. Maximum y^+ wall spacings in the turbulent region for the fine mesh are below 0.25.

Numerical Accuracy of Flow Simulations

Iterative Convergence

The simulations were marched in pseudotime until a steady state was reached. A steady state was assumed when the L2 norms of the residuals for all flow equations (mass, momentum, energy, and turbulence transport) were reduced from their initial values by at least eight orders of magnitude. The residual is defined by substituting the current solution into the steady-state form of the discretized governing equations, that is, without the time derivatives. The residuals will approach zero as a steady-state solution is reached and the current solution satisfies the discretized form of the steady equations.

The L2 residual norms of the momentum equations for the flat plate are given in Fig. 2 for all four turbulence models. The x- and y-momentum residuals are reduced by 14 orders of magnitude for each model in approximately 65,000 iterations. Similar reductions in the residuals were found for the other governing equations. Although the reduction of the residual norms to machine zero gives confidence that the iterative errors in the discrete solution are small, it is also useful to examine the iterative error directly.

The method developed by the authors in Refs. 8 and 9 has been applied to estimate the iterative error in the surface shear stress for the flat plate. The resulting iterative error estimates are presented in Fig. 3 at axial locations of 0.06 m (laminar) and 0.5 m (turbulent). The best-estimate error comes from taking the final value, after the residual norms have been reduced to machine zero, as the exact value. The local estimate at iteration n is based on the solution values at three iteration levels, n, $n + 5000$, and $n - 5000$. (See Refs. 8 and 9 for details.) Thus, the local estimate at 15,000 iterations depends on the solution values at 10,000; 15,000; and 20,000 iterations. The best estimates and local estimates for the iterative error are in agreement. The iterative errors in shear stress drop at the same rate as the L2 norms in Fig. 2. At 15,000 iterations, the L2 norms for the momentum equations has been dropped by approximately seven orders of magnitude from their initial levels, whereas the iterative errors in the shear stress are approximately 0.03% in the laminar region and 0.0004% in the turbulent region. Based on these results, a residual reduction of approximately eight orders of magnitude is enough to ensure that the iterative errors are small and may be neglected relative to the grid convergence errors discussed hereafter.

The residual norms were also examined for the sharp cone, with the results presented in Ref. 5. The two-equation turbulence models showed a 14 order of magnitude drop in y-momentum residuals, whereas the Spalart–Allmaras model[12,13] leveled off after an eight order of magnitude reduction. The reason that the residuals for the Spalart–Allmaras simulations leveled off is unknown, but based on the results presented for the flat plate, an eight order of magnitude drop is sufficient to ensure that the actual iterative errors are small.

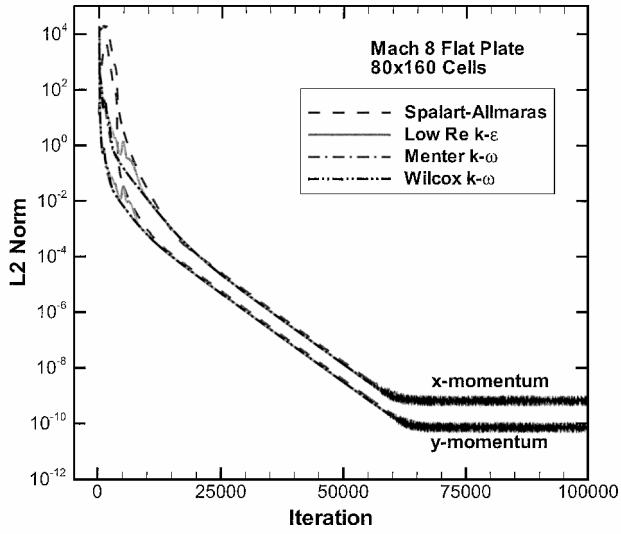

Fig. 2 Iterative convergence of the x- and y-momentum residuals for the Mach 8 flat plate.

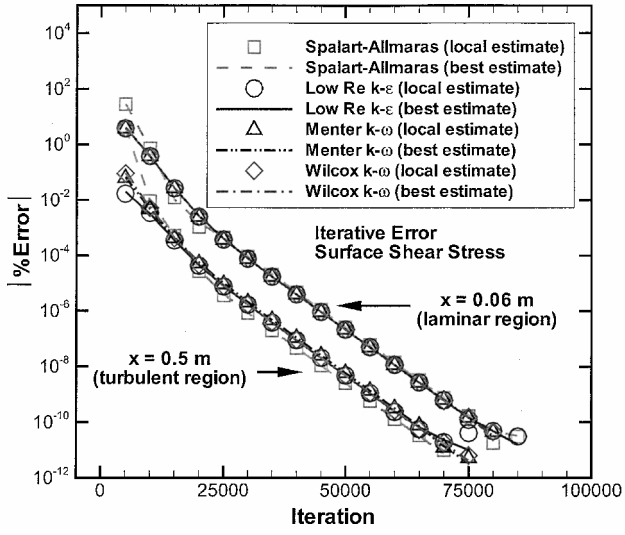

Fig. 3 Iterative error estimates in the laminar (0.06-m) and turbulent (0.5-m) regions for the Mach 8 flat plate.

Similar reductions were found for the other governing equations for this case.

Grid Convergence

Grid (or spatial) convergence has been judged from the steady-state solutions on three meshes, 1, 2, and 3 (from finest to coarsest). The Richardson extrapolation procedure (RE) (see Ref. 33) has been used to obtain a more accurate result from the relation

$$f_{\mathrm{RE}} = f_1 + (f_1 - f_2)/3 \tag{7}$$

The preceding relation assumes that the numerical scheme is second order, that both mesh levels are in the asymptotic grid convergence range, and that a mesh refinement factor of two, that is, grid doubling, is used. The accuracy of the solutions on the three meshes has been estimated using the exact solution approximated by f_{RE} that gives the solution error as

$$\%\ \text{error of}\ f_k = 100(f_k - f_{\mathrm{RE}})/f_{\mathrm{RE}} \tag{8}$$

where $k = 1, 2, 3$ is the mesh level.

If the mesh has been refined sufficiently such that the solution displays a second-order behavior, and a mesh refinement factor of two is used, then the errors on the three meshes will obey the following relationship:

$$\%\ \text{error of}\ f_1 = \%\ \text{error of}\ f_2/4 = \%\ \text{error of}\ f_3/16 \tag{9}$$

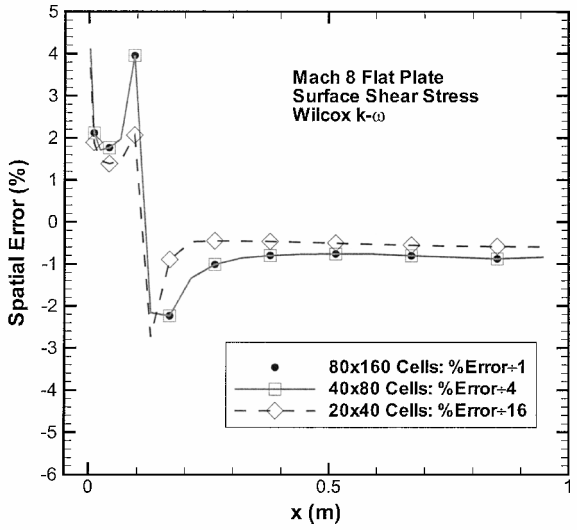

Fig. 4 Spatial error in the surface shear stress for the Mach 8 flat plate using the Wilcox k–ω turbulence model.[14]

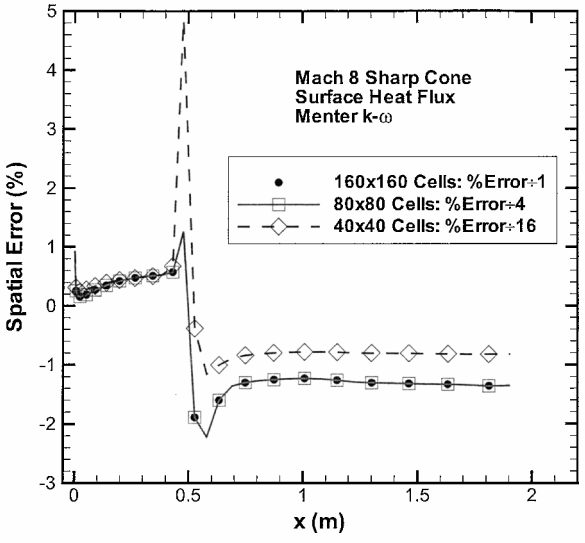

Fig. 5 Spatial error in the surface heat flux for the Mach 8 sharp cone using the Menter k–ω turbulence model.[16]

In the preceding equation, the first equality will always be satisfied when Eq. (7) is used to estimate the exact solution. The second equality will only be satisfied if all three meshes have been sufficiently refined be in the second-order asymptotic range.

Flat Plate

For the Mach 8 flat plate, the spatial discretization error in the surface shear stress was examined for each turbulence model. The normalized errors from Eq. (9) are given in Fig. 4. for the Wilcox k–ω model.[14] There is an increase in the spatial error at the transition point, but the error in the fully turbulent region is below 1%. A large error is also found at the leading-edge singularity. Beyond this point, the errors in the laminar region are below 2%. That the normalized coarse grid error distribution does not match the normalized values on the medium and fine meshes indicates that the three mesh levels are not all in the asymptotic grid convergence region. Thus, the obtained error estimates should be used with caution. Although not shown, the other two-equation turbulence models also gave spatial errors in the turbulent region of less than 1%, whereas the Spalart–Allmaras[12,13] model had errors less than 0.5% and appeared to be nearly grid asymptotic on all three grid levels that is, Eq. (9) was satisfied.

Sharp Cone

The spatial discretization error in the surface heat flux on the sharp cone is given in Fig. 5 for the Menter k–ω model.[16] The results on all three grid levels are second-order grid asymptotic in the laminar region, with fine grid heat flux errors of less than 0.5%. Again, a rise in the error is seen at the transition location. The spatial errors in the fully turbulent region are below 1.5%, with the coarse grid error failing to exhibit second-order grid asymptotic behavior. Although not shown, the low-Reynolds-number k–ε and the Wilcox k–ω two-equation turbulence models[14] also gave spatial errors near 1.5% in the turbulent region. As shown in Fig. 6, the Spalart–Allmaras model[12,13] has errors in the turbulent region of less than 0.25%. Furthermore, the normalized errors from Eq. (9) indicate that all three grid levels are in the asymptotic grid convergence range. Similar results for the surface shear stress were found using all four turbulence models.

Table 3 Freestream sensitivity of the Spalart–Allmaras model for the Mach 8 flat plate

Case	μ_t/μ	Flow
1	1×10^{-5}	T
2	0.001	T
3	0.1	T
4	1.0	T
5	10.0	T

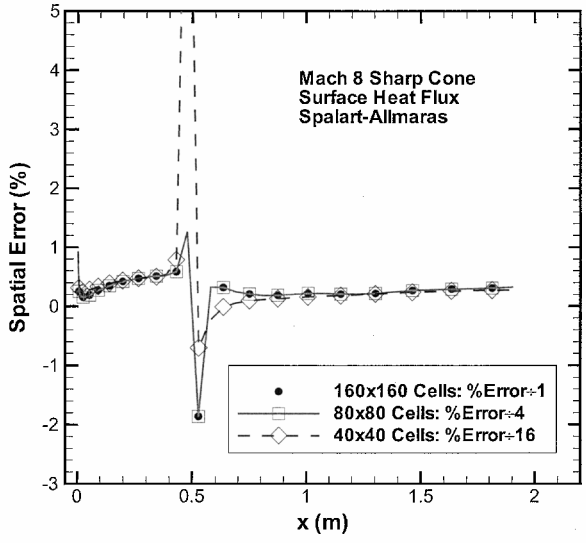

Fig. 6 Spatial error in the surface heat flux for the Mach 8 sharp cone using the Spalart–Allmaras turbulence model.[12,13]

Summary of Spatial Accuracy Study

To summarize the findings of the grid convergence study, the surface properties with the Spalart–Allmaras turbulence model[12,13] exhibited second-order grid asymptotic behavior for all three mesh levels, with fine grid errors in the turbulent region of 0.5 and 0.25% for flat plate and sharp cone, respectively. The surface properties for the two-equation models did not exhibit second-order behavior in the turbulent region on all three grids, but the estimated fine grid errors were below 1 and 1.5% for the flat plate and cone, respectively.

Freestream Turbulence Sensitivity

Turbulence models may show some sensitivity to the freestream turbulence quantities. This sensitivity can manifest in two forms: changes in the location of transition from laminar to turbulent flow and changes in the eddy viscosity levels in the turbulent region. The former may actually be a desirable characteristic when bypass transition is being modeled, whereas the latter is generally undesirable. Experimental evidence[49,50] suggests that surface properties, for example, shear stress, in the fully developed turbulent region are generally not affected by freestream turbulence intensity, at least in the case of low-speed flows.

To assess the sensitivity of the models to the freestream turbulence properties, the turbulent to laminar viscosity ratio was varied from 1×10^{-5} (case 1) to 10 (case 5), for example, see Table 3. The

Table 4 Freestream sensitivity of the low-Reynolds-number k–ε model for the Mach 8 flat plate

		T_u,%				
		A	B	C	D	E
Case	μ_t/μ	0.001	0.01	0.1	1.0	10.0
1	1×10^{-5}	L[a]	L[a]	L[a]	L[a]	L[a]
2	0.001	L[a]	L	L[a]	L[a]	L
3	0.1	L[a]	L[a]	L[a]	L[a]	L
4	1.0	L[a]	L	T	T	T
5	10.0	L[a]	L	T	T[a]	T

[a]Denotes a case that was not run.

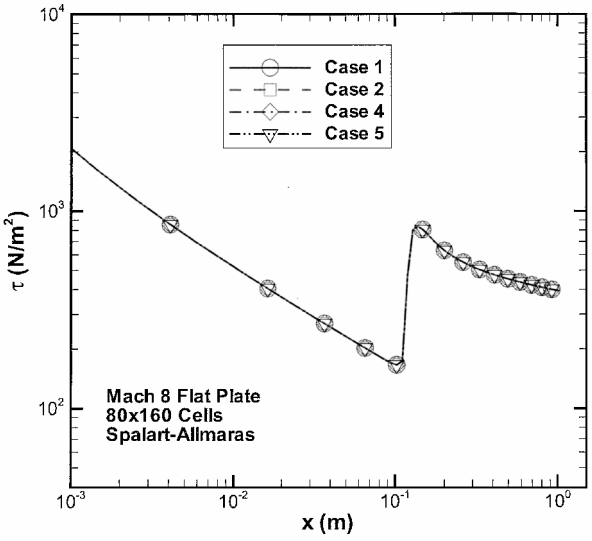

Fig. 7 Sensitivity of the Spalart–Allmaras turbulence model[12,13] to freestream turbulence levels for the Mach 8 flat plate.

turbulence intensity was varied from 0.001% (case A) to 10% (case E), for example, see Table 4. The lower turbulence intensity of case A corresponds to free flight,[51] whereas the upper limit (case E) is representative of the turbulence intensity in wind tunnels downstream of turbulence-generating screens. The physically realizable values for the turbulent to laminar viscosity ratio are more difficult to determine due to problems with direct measurements of turbulence dissipation.

To avoid running all 25 cases for each two-equation turbulence model, certain criteria were used to reduce the number of runs. For example, if two cases with the same turbulence intensity, for example, cases 1-A and 5-A, were run, and both produced laminar flow, then the cases in between, that is, 2-A, 3-A, and 4-A, were assumed to produce laminar flow and, therefore, were not run. Similarly, if the two bracketing cases produced turbulent flow with the same levels of surface shear stress or heat flux, then the cases in between were omitted. Finally, if a given case was found to be laminar, then all cases above and to the left (Table 4) were also assumed to be laminar. The flows were determined to be laminar or turbulent based on the shear stress or heat flux values downstream of the specified transition plane.

Flat Plate

The surface shear stress predictions for the Spalart–Allmaras model[12,13] on the flat plate are given in Fig. 7 for the various freestream turbulence properties (cases 1, 2, 4, and 5). All four cases resulted in turbulent flow after the transition plane. The behavior of the turbulence models can be more easily discerned by examining the shear stress in the turbulent region. This region is indicated in Fig. 8 and shows that the shear stress is insensitive to the value of eddy viscosity chosen in the freestream. These results are also presented in Table 3, where a T indicates that the shear stress downstream of the transition plane at $x = 0.5$ m was turbulent. In fact, the shear stress levels at this location for the four cases are within 0.07% for the four cases.

Table 5 Freestream sensitivity of the Menter k–ω model[16] for the Mach 8 flat plate

		T_u,%				
		A	B	C	D	E
Case	μ_t/μ	0.001	0.01	0.1	1.0	10.0
1	1×10^{-5}	L[a]	L[a]	L[a]	L[a]	L[a]
2	0.001	L[a]	L	L[a]	L[a]	L
3	0.1	L	T	T	T	T
4	1.0	L	T	T	T	T
5	10.0	L	T	T	T	T

[a]Denotes a case that was not run.

Table 6 Freestream sensitivity of the Wilcox k–ω model[14] for the Mach 8 flat plate

		T_u,%				
		A	B	C	D	E
Case	μ_t/μ	0.001	0.01	0.1	1.0	10.0
1	1×10^{-5}	L[a]	L[a]	L[a]	L[a]	L[a]
2	0.001	L[a]	L	L[a]	L[a]	L
3	0.1	L[a]	L	**411.3**	**410.7**	**410.6**
4	1.0	L	**427.2**	**416.8**	**410.8**	**410.7**
5	10.0	L	**427.6**	**425.0**	**411.9**	**411.0**

[a]Denotes a case that was not run.

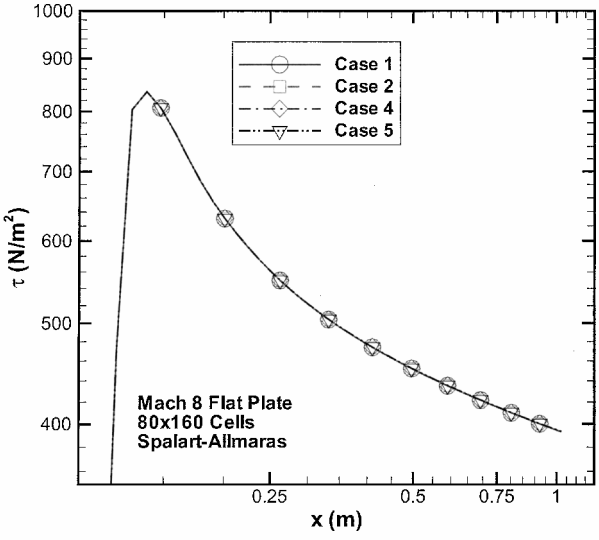

Fig. 8 Sensitivity of the Spalart–Allmaras turbulence model[12,13] to freestream turbulence levels for the Mach 8 flat plate (enlarged view).

The sensitivity to freestream turbulence levels for the low-Reynolds-number k–ε model is shown in Table 4. All cases with a freestream turbulence intensity value of less than or equal to 0.01% or eddy viscosity ratios of less than or equal to 0.1 resulted in laminar flow (L in Table 4). For all cases where the flow was turbulent, the shear stress levels at 0.5 m were within 0.01%. The behavior of the Menter k–ω model[16] is shown in Table 5. This model produced laminar flow for $T_u \leq 0.001\%$ and $\mu_t/\mu \leq 0.001$. The shear stress levels at 0.5 m were within 0.04% for all cases where turbulent flow was predicted.

The sensitivity of the Wilcox k–ω model[14] to freestream turbulence levels is given in Table 6, where the boldfaced values indicate the turbulent shear stress levels (newtons per square meter) at $x = 0.5$ m. The sensitivity to the freestream turbulence levels shows that the shear stress at this location varies by as much as 4% when the flow is turbulent. The behavior of the turbulent shear stress is shown graphically in Fig. 9. The higher levels of turbulent shear stress occur at the lower freestream ω and turbulence intensity values. Initially, it was hypothesized that higher turbulent shear stress levels may correspond to an earlier transition location on the plate. However, fully turbulent calculations did not yield a correlation between transition location and shear stress levels in the turbulent

Table 7 Freestream sensitivity of the Spalart–Allmaras model[12,13] for the Mach 8 sharp cone

Case	μ_t/μ	Flow
1	1×10^{-5}	T
2	0.001	T
3	0.1	T[a]
4	1.0	T
5	10.0	T

[a]Denotes a case that was not run.

Table 8 Freestream sensitivity of the low-Reynolds-number k–ε model for the Mach 8 sharp cone

		T_u,%				
		A	B	C	D	E
Case	μ_t/μ	0.001	0.01	0.1	1.0	10.0
1	1×10^{-5}	L[a]	L[a]	L[a]	L[a]	L[a]
2	0.001	L[a]	L	L[a]	L[a]	L
3	0.1	L[a]	L[a]	L	L	L
4	1.0	L[a]	L[a]	L	L	L
5	10.0	L[a]	L	L	T	T

[a]Denotes a case that was not run.

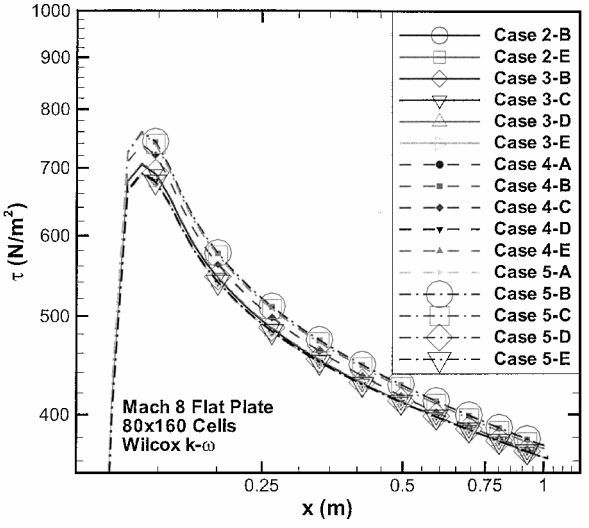

Fig. 9 Sensitivity of the Wilcox k–ω turbulence model[14] to freestream turbulence levels for the Mach 8 flat plate (enlarged view).

region. Furthermore, the experimental data of Refs. 49 and 50, although for low-speed flows, suggest that the skin-friction levels in the fully turbulent region should be insensitive to variations in the turbulence intensity. Thus, the Wilcox k–ω model's[14] sensitivity to freestream turbulence quantities is not consistent with these data.

Sharp Cone

The sensitivity of the turbulent heat flux to freestream turbulence levels for the Spalart–Allmaras model[12,13] is given in Table 7 for the sharp cone. As with the flat plate, all values of the normalized turbulent viscosity produced turbulent flow downstream of the transition plane. Furthermore, the heat flux levels at $x = 1$ m were all within 0.01%. The sensitivity of the low-Reynolds-number k–ε model to the freestream turbulence levels is given in Table 8. For this case, turbulent flow was achieved only when $\mu_t/\mu = 10$ and $T_u = 1$ or 10%. The turbulent heat flux levels at 1 m were within 0.01%.

The freestream turbulence sensitivity for the Menter k–ω model[16] is shown in Fig. 10. An enlargement of the turbulent region is given in Fig. 11 and shows that only minor variations in the turbulent heat flux occur as the freestream turbulence is varied. The sensitivity of this model is more easily seen in Table 9, where laminar flow downstream of the transition plane is observed when $T_u \leq 0.01\%$ and $\mu_t/\mu \leq 0.001$. The heating levels at $x = 1$ m are all within 0.2% when turbulent flow is predicted.

Table 9 Freestream sensitivity of the Menter k–ω model[16] for the Mach 8 sharp cone

		T_u,%				
		A	B	C	D	E
Case	μ_t/μ	0.001	0.01	0.1	1.0	10.0
1	1×10^{-5}	L[a]	L[a]	L[a]	L[a]	L[a]
2	0.001	L[a]	L	L[a]	L[a]	L
3	0.1	L[a]	L[a]	T	T[a]	T
4	1.0	L[a]	L[a]	T[a]	T	T
5	10.0	L[a]	L	T	T	T

[a]Denotes a case that was not run.

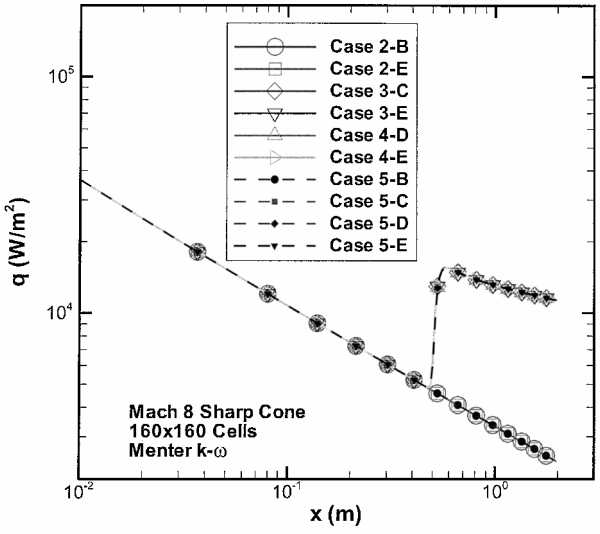

Fig. 10 Sensitivity of the Menter k–ω turbulence model[16] to freestream turbulence levels for the Mach 8 sharp cone.

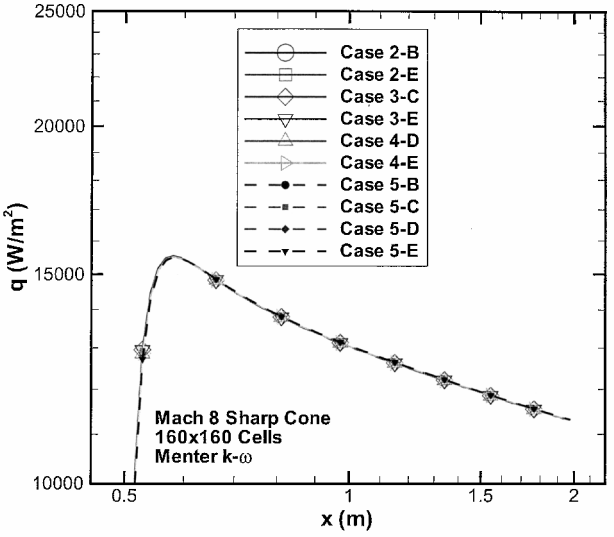

Fig. 11 Sensitivity of the Menter k–ω turbulence model[16] to freestream turbulence levels for the Mach 8 sharp cone (enlarged view).

The sensitivity of the Wilcox k–ω model[14] to the freestream turbulence values is shown graphically in Fig. 12. Similar to the Menter k–ω model,[16] this model predicts laminar flow when $T_u \leq 0.01\%$ and $\mu_t/\mu \leq 0.001$. However, there is a stronger sensitivity to the freestream turbulence levels for the Wilcox k–ω model,[14] as shown in Table 10, where heat flux levels (watts per square meter) are given when turbulent flow is predicted. The turbulent heat flux at $x = 1$ m varies by as much as 4% for the conditions examined. As in the flat plate case, this model predicts the highest turbulent heating at the lower freestream ω and turbulence intensity levels.

Table 10 Freestream sensitivity of the Wilcox k–ω model[14] for the Mach 8 sharp cone

		T_u,%				
Case	μ_t/μ	A 0.001	B 0.01	C 0.1	D 1.0	E 10.0
1	1×10^{-5}	L[a]	L[a]	L[a]	L[a]	L[a]
2	0.001	L[a]	L	L[a]	L[a]	L
3	0.1	L[a]	L[a]	**11861**	**11812**	**11812**
4	1.0	L[a]	L[a]	**12081**	**11820**	**11813**
5	10.0	L[a]	L	**12280**	**11910**	**11834**

[a]Denotes a case that was not run.

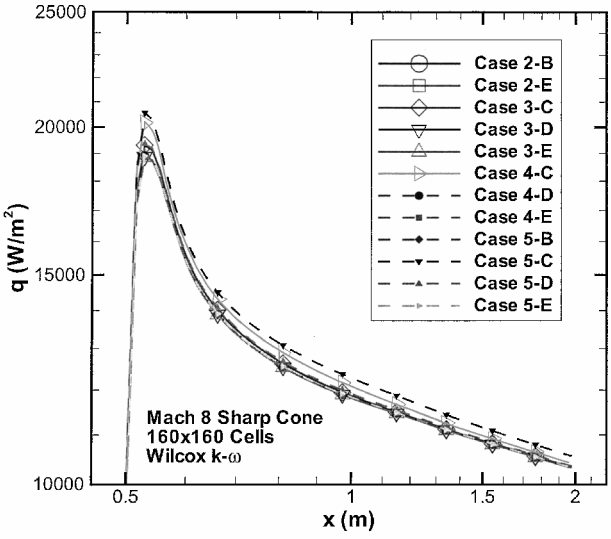

Fig. 12 Sensitivity of the Wilcox k–ω turbulence model[14] to freestream turbulence levels for the Mach 8 sharp cone (enlarged view).

Summary of the Freestream Sensitivity Study

To summarize the finding on freestream turbulence sensitivity, the Spalart–Allmaras model[12,13] was entirely insensitive to the freestream turbulence, yielding identical turbulent flow for all freestream values examined. The two-equation models showed some sensitivity in that the solutions tended to be laminar when the freestream turbulence levels were low and were turbulent when these levels were high. When the low-Reynolds-number k–ε and the Menter k–ω models[16] produced turbulent solutions, the turbulent shear stress and heating levels were within 0.2% for both the flat plate and the sharp cone. The Wilcox k–ω model,[14] however, produced turbulent surface shear stress and heating levels that varied by as much as 4% when the freestream turbulence values were varied. Furthermore, this model tended to give higher shear stress and heat flux levels at the lower freestream ω and turbulence intensity values. As expected, the freestream turbulence levels had no impact on the laminar skin friction and heating.

Wall Normal Mesh Spacing Sensitivity

The flowfield meshes for both the flat plate and the sharp cone were modified to examine the sensitivity of the turbulence models to the y^+ spacing near the wall. The fine meshes were modified only over the first 40 points, to keep the outer mesh the same. This method was chosen to isolate the y^+ sensitivity from the grid resolution sensitivity as much as possible. Within the first 40 points, the y^+ value was specified at the wall and the grid spacing at the 40th point was matched to the outer grid. A hyperbolic tangent stretching was used to vary smoothly between the wall and the outer grid.

Flat Plate

For the Mach 8 flat plate, the baseline mesh has an average y^+ wall spacing in the turbulent region of approximately 0.1. This mesh was modified as described earlier to produce meshes with y^+ spacings of 0.01, 0.25, and 1. An additional mesh was generated with a y^+ spacing of 10, which required the removal of grid points from the mesh

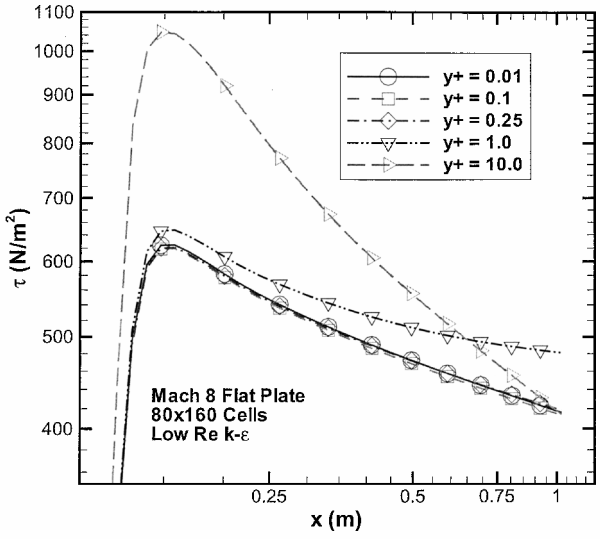

Fig. 13 Sensitivity of the low-Reynolds-number k–ε turbulence model to normal wall spacing (y^+) for the Mach 8 flat plate (enlarged view).

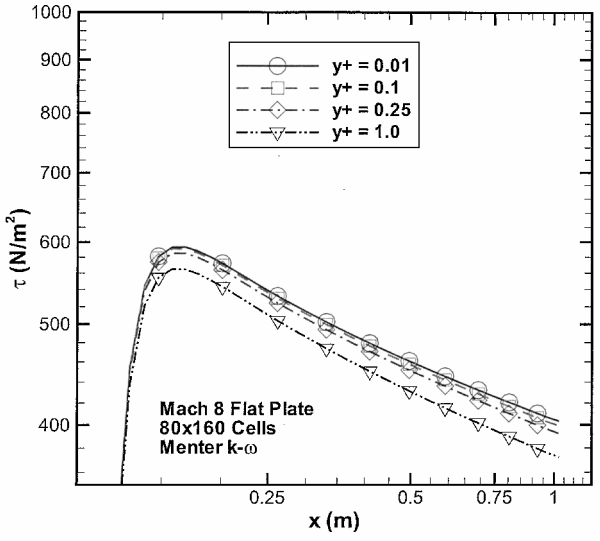

Fig. 14 Sensitivity of the Menter k–ω turbulence model[16] to normal wall spacing (y^+) for the Mach 8 flat plate (enlarged view).

to minimize large grid spacing changes. Only the low-Reynolds-number k–ε turbulence model was able to obtain a solution on this mesh, with the other three models diverging, even with a reduction in the time step.

The shear stress in the turbulent region is presented for the low-Reynolds-number k–ε model in Fig. 13. For y^+ values of 0.25 and below, this model gives consistent results for the shear stress. At the downstream end of the plate, the shear stress with $y^+ = 1$ appears to be in error by almost 15%. The results with $y^+ = 10$ greatly overpredict the shear stress immediately downstream of the transition region and clearly obtain a different slope than the smaller y^+ values.

The wall shear stress for the Menter k–ω model[16] is presented in Fig. 14 for the various y^+ wall spacings. A consistent slope is seen for all y^+ values, whereas the shear stress for the $y^+ = 1$ mesh is consistently 5% below the other curves. Although not shown, similar results were found for the Wilcox k–ω model[14] with the curves for $y^+ = 0.25$ and 0.1 even closer to that of $y^+ = 0.01$. The results for the Spalart–Allmaras model[12,13] showed good agreement for the finer y^+ spacing, and the shear stress for the $y^+ = 1$ case was only 2.5% high (not shown).

Sharp Cone

For the baseline Mach 8 sharp cone grid, the average y^+ spacing in the turbulent region was 0.25. The mesh was modified to obtain

meshes with y^+ spacings of 0.01, 0.1, and 1. An additional mesh was generated with $y^+ = 10$ by removing points from the interior portion of the grid. Again, only the low-Reynolds-number k–ε model was able to achieve a converged solution, although the results on this grid were of poor quality.

Surface heat flux distributions for the Spalart–Allmaras model[12,13] are presented in Fig. 15 for near-wall y^+ spacings of 0.01 to 1. The results are insensitive to the y^+ spacing, with maximum differences of only 2%. Sensitivity results for the Wilcox k–ω model[14] are given in Fig. 16. The solutions with the finer wall spacing are in close agreement, whereas the $y^+ = 1$ heating is approximately 6% low. Although not shown, a similar behavior is found for the Menter k–ω model,[16] with the $y^+ = 1$ heating being roughly 9% low. For the low-Reynolds-number k–ε model, the finer y^+ curves are in good agreement, whereas the $y^+ = 1$ curve is 12% high and displays a more shallow slope (not shown).

Summary of the Wall Spacing Study

The Spalart–Allmaras model[12,13] was shown to be the least sensitive to the wall y^+ spacing, with differences of less than 2.5% in the turbulent region for both cases. The k–ω models were mildly sensitive to the wall y^+, with the Wilcox k–ω model[14] giving differences of less than 6% for both cases and the Menter k–ω model[16] giving differences of 5 and 9% for the flat plate and cone, respectively. The k–ε model was the only model that ran for the $y^+ = 10$ case; however, the results for this model were poor for both $y^+ = 10$ and 1.

Model Validation

Flat Plate

For the baseline freestream conditions, the transitional flow over a flat plate at Mach 8 has been calculated with the SACCARA code and compared to the accurate laminar and turbulent results obtained for this case by Van Driest.[1,2] The transition location was arbitrarily specified at $x_t = 0.12$ m for this case. Skin-friction profiles have been obtained using all four turbulence models and are presented in Fig. 17. The Reynolds number based on an axial coordinate is used for the abscissa because typical boundary-layer properties such as momentum thickness are difficult to compute for Navier–Stokes codes. All simulations correctly predict the laminar skin friction, according to Van Driest,[1] upstream of the transition plane. Details of the turbulent region are shown in Fig. 18 for each model. The results appear to reach an approximately constant error relative to the Van Driest correlation[2] by the end of the plate. At this location, the Wilcox k–ω model[14] underpredicts the Van Driest[2] curve by 6.7%, whereas the Spalart–Allmaras,[12,13] Menter k–ω (Ref. 16), and low-Reynolds-number k–ε overpredict the skin friction by 1.4, 3.1, and 6.3%, respectively. The Van Driest correlation,[2] as discussed in the preceding section, is based on theory as well as a large amount

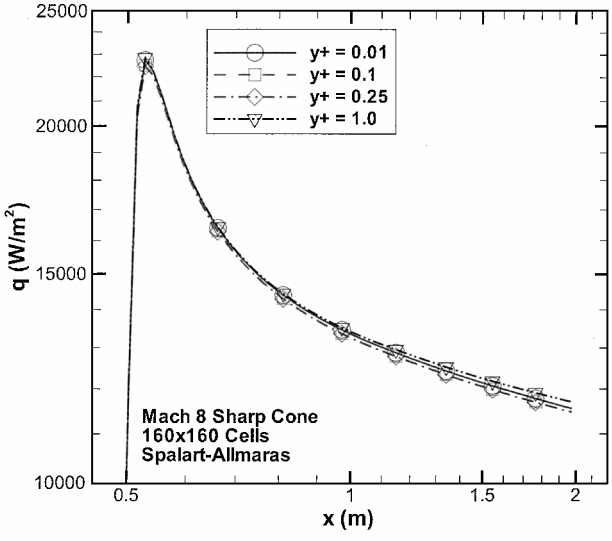

Fig. 15 Sensitivity of the Spalart–Allmaras turbulence model[12,13] to normal wall spacing (y^+) for the Mach 8 sharp cone (enlarged view).

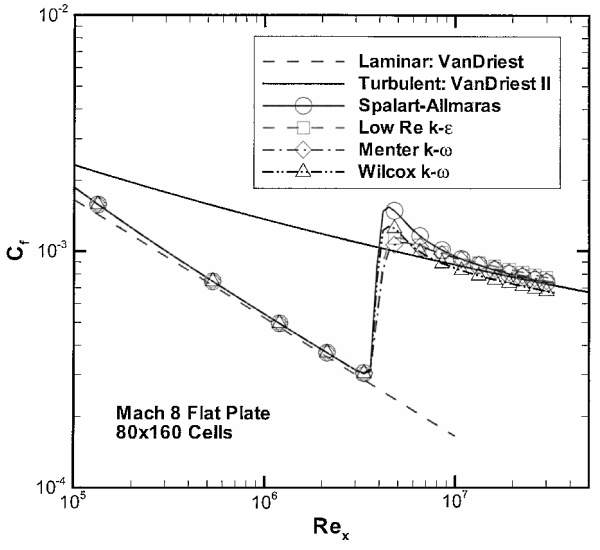

Fig. 17 Comparison of the turbulence models to the Van Driest correlations[1,2] for the Mach 8 flat plate.

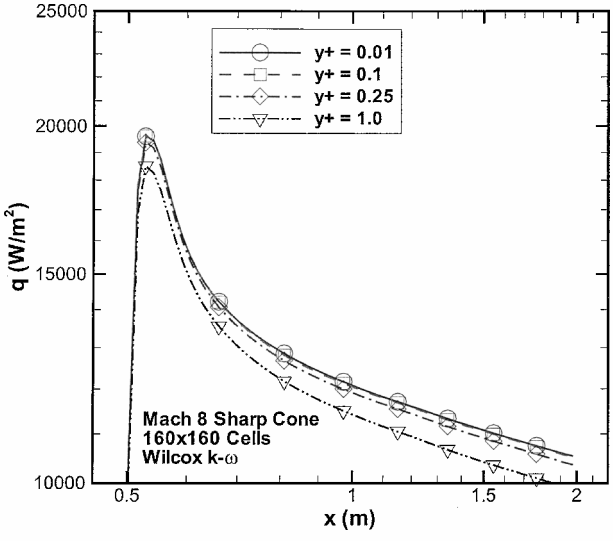

Fig. 16 Sensitivity of the Wilcox k–ω turbulence model[14] to normal wall spacing (y^+) for the Mach 8 sharp cone (enlarged view).

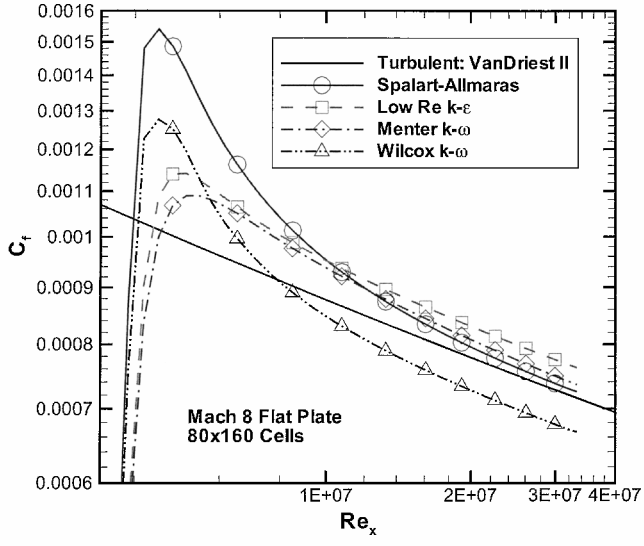

Fig. 18 Comparison of the turbulence models to the Van Driest correlations[1,2] for the Mach 8 flat plate (enlarged view).

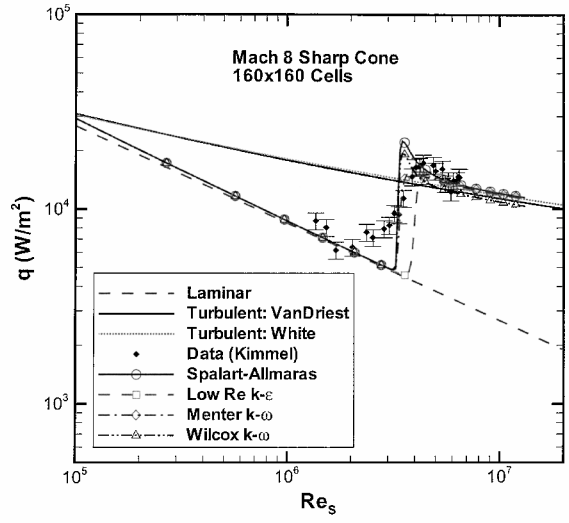

Fig. 19 Comparison of the turbulence models to the Van Driest correlations[3,4] for the Mach 8 sharp cone.

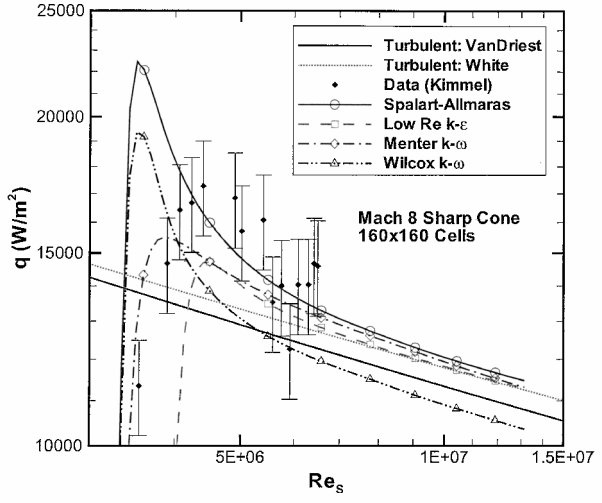

Fig. 20 Comparison of the turbulence models to the Van Driest correlations[3,4] for the Mach 8 sharp cone (enlarged view).

of experimental data. Squire[52] estimates that the accuracy of this relationship is within ±3%. Accounting for the grid convergence errors, the skin-friction predictions from the Spalart–Allmaras[12,13] and Menter k–ω models[16] are within the error tolerances, whereas the low-Reynolds-number k–ε and Wilcox k–ω models[14] are not.

Sharp Cone

For the baseline freestream conditions, the transitional flow over a sharp cone at Mach 8 has been simulated. Surface heating results vs surface distance Reynolds number are presented in Fig. 19 for the four turbulence models along with laminar boundary-layercode results, turbulent Van Driest cone theory,[3] and White's turbulent cone rule[4] (see Ref. 5 for details). In addition, experimental data are taken from Ref. 27 and include the conservative 10% error bounds suggested by Kimmel. Note that these data are presented in terms of the surface distance Reynolds number based on the freestream conditions, whereas the Reynolds number based on edge conditions was used in Fig. 5 of Ref. 27. Although the surface heating predictions in the transitional region do not match the experimental data, the predictions in both the laminar and turbulent regions are generally within the experimental error bounds. Note that the low-Reynolds-number k–ε model gives transition slightly downstream of the specified transition point for the chosen freestream turbulence values.

An enlarged view of the turbulent heating region is presented in Fig. 20. At the end of the cone, the two theoretical correlations agree to within 4%. This difference is well within the accuracy of

Table 11 Summary of turbulence mode assessment for zero pressure gradient boundary layer flows

	Model			
Criteria	Spalart–Allmaras[12,13]	Low-Reynolds-number k–ε	Menter k–ω (Ref. 16)	Wilcox k–ω (Ref. 14)
Freestream turbulence sensitivity	★★★★	★★★	★★★	★
Wall y^+ sensitivity	★★★★	★	★★★	★★★
Grid resolution sensitivity	★★★★	★★★	★★★	★★★
Model validation: flat plate	★★★★	★★	★★★★	★★
Model validation: sharp cone	★★★	★★★	★★★	★★★

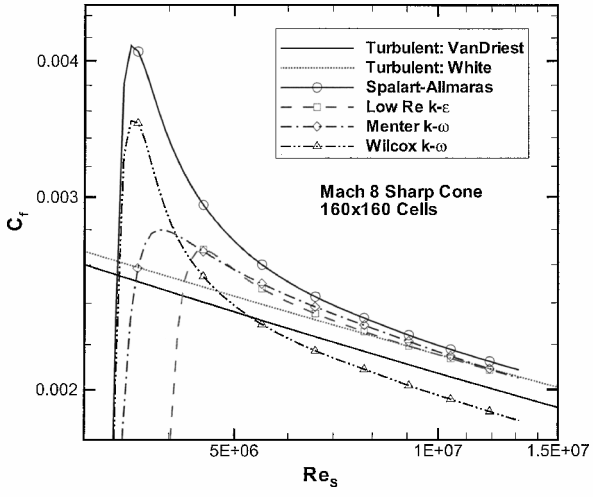

Fig. 21 Comparison of the turbulence models to the Van Driest correlations[3,4] for the Mach 8 sharp cone (enlarged view).

the correlations, which is estimated to be approximately ±5–10%. When the theoretical value is taken to be the average of these two curves, the Wilcox k–ω model[14] is roughly 5.7% below the theory at the end of the cone. Both the Menter k–ω model[16] and the low-Reynolds-number k–ε model predict heating values approximately 2.5% high, whereas the Spalart–Allmaras model[12,13] is 4.3% high. When the grid convergence errors discussed earlier are accounted for, all of the turbulence models are well within the estimated error bounds. The skin-friction results for the sharp cone show a high degree of similarity to the heating results, with an enlargement of the turbulent region given in Fig. 21.

The foregoing model assessment results are summarized in Table 11. For each category, the models are given ratings from one star to four stars, with one being poor and four being excellent.

Summary

A turbulence model assessment methodology was developed that includes documentation procedures, solution accuracy assessment, model sensitivity, and model validation. This methodology was applied to the Mach 8, perfect gas flow over a flat plate and a sharp cone using four turbulence models: the one-equation eddy viscosity transport model of Spalart–Allmaras,[12,13] a low-Reynolds-number k–ε model, the Menter k–ω model,[16] and the Wilcox k–ω model.[14]

The numerical accuracy of the surface shear stress and heat flux was examined for the various models. Iterative convergence was demonstrated by reducing the L2 norms of the governing equations by at least eight orders of magnitude for all equations. Surface properties in the laminar regions were second-order grid asymptotic, with errors below 2% for both cases. The surface shear stress for the flat plate in the fully turbulent region was nearly grid asymptotic,

with error estimates below 1% for the two-equation models. The surface heat flux in the fully turbulent region for the cone had error estimates below 1.5% for the two-equation models; however, these results were not fully second-order asymptotic on all three meshes. The Spalart–Allmaras one-equation model[12,13] gave results in the turbulent region that were fully second-order grid asymptotic for both cases. For this model, the grid convergence errors in shear stress for the flat plate were within 0.5%, and the heat flux errors for the sharp cone were within 0.25%.

The sensitivity of the surface properties to the freestream turbulence levels was examined. The Spalart–Allmaras model[12,13] showed no sensitivity because all freestream turbulence levels produced identical turbulent results downstream of the transition point. The two-equation models often gave laminar flow downstream of the transition point for the lower levels of freestream turbulence. When turbulent flow was predicted, the low-Reynolds-number k–ε and Menter k–ω (Ref. 16) models produced the same levels of shear stress and heating in the fully turbulent region, regardless of the freestream turbulence levels. The Wilcox k–ω model,[14] however, was sensitive to the freestream turbulence levels, with turbulent shear stress and heat flux results varying by as much as 4%. In addition, this model tended to produce higher turbulent shear stress and heating values at the lower ω and turbulence intensity values. For some of the turbulence models, unrealistically high freestream turbulence levels were required to obtain turbulent flow.

The sensitivity of the surface properties to the y^+ normal spacing at the wall was also examined. For the Spalart–Allmaras model,[12,13] when the y^+ wall spacing was varied between 0.01 and unity, the surface properties varied by less than 2.5% for both flow cases. The Menter k–ω (Ref. 16) and Wilcox k–ω (Ref. 14) models produced y^+ variations in surface properties within 9 and 6%, respectively. The low-Reynolds-number k–ε model was sensitive to the y^+ wall spacing, with y^+ variations between 0.01 and unity, yielding surface property variations as high as 15%.

For the compressible flat plate, the turbulent shear stress correlations of Van Driest[2] are well established and are accurate to within ±3% (see Ref. 52). The wall shear stress from the Spalart–Allmaras[12,13] and Menter k–ω (Ref. 16) models were within the uncertainty of the correlations when the grid convergence errors were taken into account, whereas the low-Reynolds-number k–ε and Wilcox k–ω (Ref. 14) models were not. The surface property correlations for the sharp cone are not as well established and are estimated to only be accurate within ±5–10%. All four turbulence models gave surface heat flux results within these broad uncertainty bands. Further work is required to reduce the uncertainty in the sharp cone correlations to improve the validation of the models for this flow.

Overall, the Spalart–Allmaras model[12,13] excels in almost every model assessment category, whereas the Menter k–ω model[16] also performs quite well. The low-Reynolds-number k–ε model showed a strong sensitivity in the surface properties to the y^+ wall spacing; however, note that the incompressible form of the turbulent kinetic energy production term was employed. The Wilcox k–ω model[14] showed a strong sensitivity to the freestream turbulence levels. These two models also failed to give shear stress results within the correlation uncertainty for the flat plate, even after the grid convergence errors were taken into account.

Acknowledgments

This work was supported by Sandia National Laboratories and the Department of Energy's Accelerated Strategic Computing Initiative. Sandia is a multiprogram laboratory operated by Sandia Corp., a Lockheed Martin Company, for the U.S. Department of Energy under Contract DE-AC04-94AL85000. The authors thank Kambiz Salari of Lawrence Livermore National Laboratory for his helpful discussions on turbulence model assessment and Curtis Ober of Sandia National Laboratories for his careful review of the manuscript.

References

[1]Van Driest, E. R., "Investigation of Laminar Boundary Layer in Compressible Fluids Using the Crocco Method," NACA TN-2597, Jan. 1952.

[2]Van Driest, E. R., "Problem of Aerodynamic Heating," *Aeronautical Engineering Review*, Vol. 15, No. 10, 1956, pp. 26–41.

[3]Van Driest, E. R., "Turbulent Boundary Layer on a Cone in a Supersonic Flow at Zero Angle of Attack," *Journal of the Aeronautical Sciences*, Vol. 19, No. 1, 1952, pp. 55–57.

[4]White, F. M., *Viscous Fluid Flow*, 1st ed., McGraw–Hill, New York, 1974, pp. 647–648.

[5]Roy, C. J., and Blottner, F. G., "Further Assessment of One- and Two-Equation Turbulence Models for Hypersonic Transitional Flows," AIAA Paper 2001-0210, Jan. 2001.

[6]Marvin, J. G., "Perspective on Computational Fluid Dynamics Validation," *AIAA Journal*, Vol. 33, No. 10, 1995, pp. 1778–1787.

[7]Marvin, J. G., and Huang, G. P., "Turbulence Modeling—Progress and Future Outlook," *Computational Fluid Dynamics Review 1998*, Vol. 2, edited by M. Hafez and K. Oshima, World Scientific, Singapore, Republic of Singapore, 1998, pp. 891–906.

[8]Roy, C. J., and Blottner, F. G., "Assessment of One- and Two-Equation Turbulence Models for Hypersonic Transitional Flows," AIAA Paper 2000-0132, Jan. 2000.

[9]Roy, C. J., and Blottner, F. G., "Assessment of One- and Two-Equation Turbulence Models for Hypersonic Transitional Flows," *Journal of Spacecraft and Rockets*, Vol. 38, No. 5, 2001, pp. 699–710.

[10]Wong, C. C., Blottner, F. G., Payne, J. L., and Soetrisno, M., "Implementation of a Parallel Algorithm for Thermo-Chemical Nonequilibrium Flow Solutions," AIAA Paper 95-0152, Jan. 1995.

[11]Wong, C. C., Soetrisno, M., Blottner, F. G., Imlay, S. T., and Payne, J. L., "PINCA: A Scalable Parallel Program for Compressible Gas Dynamics with Nonequilibrium Chemistry," Sandia National Lab., Rept. SAND 94-2436, Albuquerque, NM, April 1995.

[12]Spalart, P. R., and Allmaras, S. R., "A One-Equation Turbulence Model for Aerodynamic Flows," AIAA Paper 92-0439, Jan. 1992.

[13]Spalart, P. R., and Allmaras, S. R., "A One-Equation Turbulence Model for Aerodynamic Flows," *La Recherche Aerospatiale*, No. 1, 1994, pp. 5–21.

[14]Wilcox, D. C., *Turbulence Modeling for CFD*, 2nd ed., DCW Industries, La Canada, CA, 1998, pp. 119–122.

[15]Nagano, Y., and Hishida, M., "Improved Form of the k–ε Model for Wall Turbulent Shear Flows," *Journal of Fluids Engineering*, Vol. 109, No. 2, 1987, pp. 156–160.

[16]Menter, F. R., "Two-Equation Eddy-Viscosity Turbulence Models for Engineering Applications," *AIAA Journal*, Vol. 32, No. 8, 1994, pp. 1598–1605.

[17]Wilcox, D. C., "Reassessment of the Scale Determining Equation for Advanced Turbulence Models," *AIAA Journal*, Vol. 26, No. 11, 1988, pp. 1299–1310.

[18]Huang, P. G., Bradshaw, P., and Coakley, T. J., "Turbulence Models for Compressible Boundary Layers," *AIAA Journal*, Vol. 32, No. 4, 1994, pp. 735–740.

[19]Kral, L. D., Mani, M., and Ladd, J. A., "Application of Turbulence Models for Aerodynamic and Propulsion Flowfields," *AIAA Journal*, Vol. 34, No. 11, 1996, pp. 2291–2298.

[20]Bertin, J. J., Martellucci, A., and Neumann, R. D., "Developing a Data Base for the Calibration and Validation of Hypersonic CFD Codes—Sharp Cones," AIAA Paper 93-3044, July 1993.

[21]Chien, K.-Y., "Hypersonic, Turbulent Skin-Friction and Heat-Transfer Measurements on a Sharp Cone," *AIAA Journal*, Vol. 12, No. 11, 1974, pp. 1522–1526.

[22]Desideri, J.-A., Glowinski, R., and Periaux, J., (eds.), *Hypersonic Flows for Reentry Problems*, Vols. 1 and 2, Springer-Verlag, Berlin, 1991, pp. 214, 215.

[23]Lin, L. B., and Harvey, J. K., "Experimental Study of the Hypersonic Turbulent Boundary Layer on a Cold Slender Cone," *Journal of Thermophysics and Heat Transfer*, Vol. 3, No. 2, 1989, pp. 105–111.

[24]Hillier, R., Kirk, D. C., Sell, M., and Soltani, S., "Studies of Hypersonic Viscous Flows," *Theoretical and Experimental Methods in Hypersonic Flows*, CP 514, AGARD, 1992, pp. 32-1–32-11.

[25]Chen, F.-J., Malik, M. R., and Beckwith, I. E., "Boundary-Layer Transition on a Cone and Flat Plate at Mach 3.5," *AIAA Journal*, Vol. 27, No. 6, 1989, pp. 687–693.

[26]Kimmel, R. L., "Experimental Transition Zone Lengths in Pressure Gradient in Hypersonic Flow," *Transitional and Turbulent Compressible Flows 1993*, edited by L. D. Kral and T. A. Zang, Fluid Engineering Div., Vol. 151, American Society of Mechanical Engineers, New York, 1993, pp. 117–127.

[27]Kimmel, R. L., "The Effects of Pressure Gradients on Transition Zone Length in Hypersonic Boundary Layers," *Journal of Fluids Engineering*, Vol. 119, No. 1, 1997, pp. 36–41.

[28]Zoby, E. V., and Sullivan, E. M., "Correlation of Free-Flight Turbulent Heat-Transfer Data from Axisymmetric Bodies with Compressible Flat-Plate Relationships," NASA TN D-3802, Jan. 1967.

[29]Zoby, E. V., and Graves, R. A., "Comparison of Turbulent Prediction Methods with Ground- and Flight-Test Heating Data," *AIAA Journal*, Vol. 15, No. 7, 1977, pp. 901, 902.

[30]Moore, J. G., and Moore, J., "Realizeability in Two-Equation Turbulence Models," AIAA Paper 99-3779, June 1999.

[31]Roache, P. J., "Ch. 3: A Methodology for Accuracy Verification of Codes: The Method of Manufactured Solutions," *Verification and Validation in Computational Science and Engineering*, Hermosa, Albuquerque, NM, 1998, pp. 65–90.

[32]Salari, K., and Knupp, P., "Code Verification by the Method of Manufactured Solutions," Sandia National Labs., Rept. SAND2000-1444, Albuquerque, NM, June 2000.

[33]Roache, P. J., "Perspective: A Method for Uniform Reporting of Grid Refinement Studies," *Journal of Fluids Engineering*, Vol. 116, No. 3, 1994, pp. 405–413.

[34]Carpenter, M. H., and Casper, J. H., "Accuracy of Shock Capturing in Two Spatial Dimensions," *AIAA Journal*, Vol. 37, No. 9, 1999, pp. 1072–1079.

[35]Roy, C. J., "Grid Convergence Error Analysis for Mixed-Order Numerical Schemes," AIAA Paper 2001-2606, June 2001.

[36]Oberkampf, W. L., Aeschliman, D. P., Henfling, J. F., and Larson, D. E., "Surface Pressure Measurements for CFD Code Validation in Hypersonic Flow," AIAA Paper 95-2273, June 1995.

[37]Harten, A., "On a Class of High Resolution Total-Variation-Stable Schemes," *SIAM Journal on Numerical Analysis*, Vol. 21, No. 1, 1984, pp. 1–23.

[38]Yee, H. C., "Implicit and Symmetric Shock Capturing Schemes," NASA TM-89464, May 1987.

[39]Roe, P. L., "Approximate Riemann Solvers, Parameter Vectors, and Difference Schemes," *Journal of Computational Physics*, Vol. 43, No. 2, 1981, pp. 357–372.

[40]Yoon, S., and Jameson, A., "An LU-SSOR Scheme for the Euler and Navier–Stokes Equations," AIAA Paper 87-0600, Jan. 1987.

[41]Yoon, S., and Kwak, D., "Artificial Dissipation Models for Hypersonic External Flow," AIAA Paper 88-3708, July 1988.

[42]Peery, K. M., and Imlay, S. T., "An Efficient Implicit Method for Solving Viscous Multi-Stream Nozzle/Afterbody Flow Fields," AIAA Paper 86-1380, June 1986.

[43]Payne, J. L., and Hassan, B., "Massively Parallel Computational Fluid Dynamics Calculations for Aerodynamics and Aerothermodynamics Applications," *Proceedings of the 1998 High Performance Computing and Communications Program/Computational AeroSciences Workshop*, NASA CP-1999-208757, Jan. 1999, pp. 111–116.

[44]Hassan, B., Kuntz, D. W., and Potter, D. L., "Coupled Fluid/Thermal Prediction of Ablating Hypersonic Vehicles," AIAA Paper 98-0168, Jan. 1998.

[45]Kuntz, D. W., Hassan, B., and Potter, D. L., "Predictions of Ablating Hypersonic Vehicles Using an Iterative Coupled Fluid/Thermal Approach," *Journal of Thermophysics and Heat Transfer*, Vol. 15, No. 2, 2001, pp. 129–139.

[46]Roy, C. J., McWherter-Payne, M. A., and Oberkampf, W. L., "Verification and Validation for Laminar Hypersonic Flowfields," AIAA Paper 2000-2550, June 2000.

[47]*U.S. Standard Atmosphere*, National Oceanic and Atmospheric Administration, NASA, and U.S. Air Force, NOAA-S-T-76-1562, Washington, DC, Oct. 1976.

[48]Keyes, F. G., "A Summary of Viscosity and Heat-Conduction Data for He, A, H_2, O_2, CO, CO_2, H_2O, and Air," *Transactions of the American Society of Mechanical Engineers*, July 1951, pp. 589–596.

[49]Craft, T. J., Launder, B. E., and Suga, K., "Prediction of Turbulent Transitional Phenomena with a Nonlinear Eddy-Viscosity Model," *International Journal of Heat and Fluid Flow*, Vol. 18, No. 1, 1997, pp. 15–28.

[50]Cebici, T., and Bradshaw, P., "Uncoupled Turbulent Boundary Layers," *Physical and Computational Aspects of Convective Heat Transfer*, Springer-Verlag, New York, 1984, p. 173.

[51]Reed, H. L., Kimmel, R., Schneider, S., and Arnal, D., "Drag Prediction and Transition in Hypersonic Flow," AIAA Paper 97-1818, June 1997.

[52]Squire, L. C., "The Accuracy of Flat Plate, Turbulent Skin Friction at Supersonic Speeds," *Aeronautical Journal*, Vol. 104, No. 1036, 2000, pp. 257–263.

B. Hassan
Associate Editor